Geomechanical characterization and analysis of the Upper Cretaceous Flysch materials found in the Basque Arc Alpine region

Julio Garzón-Roca[a,*], F. Javier Torrijo[b,c], Julio Company[b], Guillermo Cobos[b]

[a] Department of Civil and Environmental Engineering, University of Surrey, Guildford GU2 7XH, UK.

[b] Department of Geotechnical Engineering, Universitat Politècnica de València, Camino de Vera s/n, 46022, Valencia, Spain.

[c] Research Centre PEGASO, Universitat Politècnica de València, Camino de Vera s/n, 46022, Valencia, Spain.

**Corresponding author*. Tel.: +34 963 877 582; fax: +34 963 877 569; e-mail address: jugarro@upv.es

Abstract

Flysch materials are one of the most challenging geological materials and often give rise to slope instability problems. Due to its natural heterogeneity, geomechanical characterization of Flysch materials is somewhat difficult. The Spanish Basque Arc Alpine region is a very well-known location for flysch materials. In this paper, an area of approximately 100 km^2 in the region is intensively studied and their flysch materials geomechanically characterized. A total of 33 locations are investigated by a broad geological-geotechnical investigation, involving petrographic analyses, geomechanical stations, boreholes and mechanical laboratory tests. In addition, a slope inventory was carried out to assess the situation in the existing slopes in the area. Characterization of materials is carried out in terms of *RQD*, *RMR* and *GSI* as well as using the Hoek-Brown failure criterion. Different correlations are assessed, establishing their appropriateness for estimating the mechanical parameters of a flysch material rock mass.

Keywords: Alpine regions; Flysch materials; Geomechanical characterization; Geological Strength Index; Uniaxial compressive strength; Shear strength parameters

1. Introduction

Flysch is one of the most problematic geological materials. The presence of flysch materials is often the source of slope instability problems, with accidents being reported during work construction and over the duration of a structure's service life (Morales et al. 2004; Marinos et al. 2006, 2011; Gong et al. 2010; Fortsakis et al. 2012; Akin 2013; Cano and Tomás 2013; Vassilis 2019). In the field of geotechnical engineering, flysch materials commonly include other flysch-like sedimentation deposits, i.e. complex lithological sequences mainly composed of turbidites, slumps and olitostromes (Kuenen and Migliorini 1950; Bouma 1962; Sanders 1965; Hoedemaeker 1973; Mutti et al. 2003, 2009; Saroglou et al. 2019).

Geomechanical characterization of rock masses has been an important topic in geotechnical engineering since its development. Several geomechanical indices, such as Rock Mass Rating (RMR) (Bieniaswki 1989) or Rock Mass Quality (Q) (Barton et al. 1974), were developed to help engineers tackle typical geotechnical issues such as slope stabilization and tunnel construction. However, many of them were developed for igneous rock masses, which generally present prismatic block shapes. Conversely, flysch materials are characterized by tabular and planar block shapes. Some proposals have been put forward for heterogenic materials (like flysch), such as the work conducted by Popiolek et al. (1993), Ünal (1996) Wu et al. (2017) and Saroglou et al. (2019). Similarly, Morales et al. (2004) studied flysch materials in the Basque Arc (Basque-Cantabrian Basin, North East of Spain) and proposed a classification of flysch rock masses in terms of the uniaxial compressive strength of the intact rock and the Geological Strength Index (GSI) calculated according to Hoek (2000), Marinos et al. (2001) and Marinos (2019).

This paper is focused on the study and characterization of the flysch materials found near Astigarraga, a village located close to the city of San Sebastian (Basque Country, Spain), where a railway line has been proposed. Flysch materials in this area correspond to the Upper Cretaceous and are identified as "Upper Cretaceous Flysch" on regional studies (EVE 1998). A broad geological-geotechnical investigation was performed, including boreholes, geomechanical stations and an inventory slope. Laboratory tests were also carried out to achieve more accurate petrographic and mechanical descriptions. It should be noted that, although the railway construction will involve some dynamic loading that can affect the mechanical behavior of the rock masses, such effects were considered to be outside the scope of this work and so were not taken into account.

Although the area under study belongs to the Basque Arc, unlike Morales et al. (2004), who examined a total of 99 locations spread over 3000 km^2, in this paper the investigation focuses on a detailed area, with a total of 33 locations assessed over approximately 100 km^2. Besides this, the area explored corresponds to a place where no samples were studied by Morales et al. (2004). Thus, this paper aims to validate the work of Morales et al. (2004) and enable its extension to all flysch materials. In addition, the mechanical behavior of such materials is studied, assessing the degree of suitability of the use of different correlations and approximations to estimate mechanical parameters.

2. Geographical and Geological Situation

The study area is located in the Basque-Cantabrian Basin (BCB), located on the northern margin of the Iberian Peninsula, Spain (**Fig. 1**). The Basque-Cantabrian Basin is an inverted Mesozoic extensional basin, connecting the Pyrenees in the East with the Cantabrian Mountains in the West. At present, it is considered part of the Pyrenean-Cantabrian belt, extending for more than 1000 km from the Mediterranean border of France and Spain to the western end of the Iberian Atlantic coast (Tugend et al. 2014).

The development of the Basque-Cantabrian Basin is linked to the opening of the North Atlantic Ocean and the formation of the Bay of Biscay in the Mesozoic (Le Pichon et al. 1971; Ziegler 1988; García-Mondéjar et al. 1996; Roca et al. 2011). The basin underwent two major rifting episodes during the Permian-Triassic and the Late Jurassic and high subsidence rates occurred during the Cretaceous. Therefore, the sedimentary record of the BCB is characterized by several kilometers of Mesozoic to Paleogene sedimentary sequences, composed of coastal siliciclastic and marine carbonate deposits (García-Mondéjar et al. 1996).

The sedimentary BCB infill was thrusted and folded (i.e. uplifted) during the Alpine orogeny compression (Late Cretaceous to Middle Miocene) as a consequence of the collision between the Afro-Iberian and the Eurasian plates, resulting in a basin inversion (Cámara 1997; Gómez et al. 2002; Tugend et al. 2014). The most intensely deformed area of the BCB is the Basque Arc (Feuillee and Rat 1971), which is a north and south-verging thrust belt characterized by the arched shape of its structural elements. This complex area, placed between the Basque Paleozoic Massif to the East and the Bay of Biscay coastline (**Fig. 1**), is composed of a number of vergent thrust sheets, strike-slip sub-vertical faults and major fold structures. The latter include (from N to S) the North-Biscay anticlinorium, the Biscay synclinorium and the Bilbao anticlinorium (Ábalos et al. 2008).

The 8 km-long projected stretch of the high-speed Vitoria-Bilbao-San Sebastian railway line will connect the Basque cities of Hernani and Renteria, through the area surrounding the village of Astigarraga (**Fig. 2**). The railway track will run through a geologically diverse area located between the eastern end of the North Biscay anticlinorium of the Basque Arc and the Cinco Villas Massif. Earthworks related to the railway construction will be affected by the varied sedimentary lithologies present, which reflect the palaeogeographic evolution of the Bay of Biscay basin. These comprise: Upper Triassic red clays and evaporites of the Keuper facies, with sub-volcanic intrusions (dolerites) deposited in continental environments during the rifting phase; Lower Jurassic limestones, dolomites and marly limestones deposited on a shallow marine platform during the opening of the North Atlantic Ocean; Aptian to Early Albian sequences of Urgonian reef limestones with intercalations of detrital deposits of sandstones, clays and marls; sediments of the supra-Urgonian complex (Upper Albian to Lower Cenomanian), composed of sandy calcarenites, sandstones and conglomerates from fluvial to transitional environments (Oiartzum Formation); Campanian to Lower Paleogene turbiditic successions from a deep, open marine environment (calcareous and siliciclastic flysch facies); and, lastly, the overlying Quaternary fluvial deposits of the Urumea river and coarse-grained colluvial sediments from bedrock weathering (see **Fig. 2**).

This research is focused on materials belonging to the Upper Cretaceous turbidite sequence or "Upper Cretaceous Flysch" on regional studies (EVE 1998). That Upper Cretaceous turbidite sequence consists of more than 700 m interbedded marls and marly limestones, becoming a more quartz-rich facies towards the upper part of the section (due to the increasing presence of clastic turbidites, resulting from density currents). According to such noticeable variations in lithological composition, two different units were differentiated: the Lower Itziar Formation, informally named "Calcareous Flysch" and the Upper Aguinaga Formation or "Siliciclastic Flysch" (Baceta et al. 2011). These sedimentary successions were deposited in the flysch trough of the Basque-Cantabric Basin (Mary et al. 1991; Pujalte et al. 1995). This interplate trough formed from smaller basins generated in previous rifting stages at the start of the Pyrenean convergence (Pujalte et al. 1998). Limestones, marls and occasional turbidites were deposited in a hemipelagic setting with an estimated water depth of 800 to 1500 m during an interval of increased subsidence. The Upper Maastrichtian to Paleocene was characterized by relative tectonic stability and only slight subsidence (Pujalte et al. 1998). The complete sequence has been dated as Cenomanian to Lower Maastrichtian in age (Eve 1988; Mathey 1982; Morales et al. 2004).

3. Materials and Methods

3.1. Geological-geotechnical investigation

A geological-geotechnical investigation including 24 petrographic analyses, 33 geomechanical stations and 40 boreholes was carried out. It should be noted that other tests were also conducted but only those relevant to the topic developed in this article are considered here. A total of 33 locations were investigated (see **Fig. 2**), of which 18 belonged to the upper flysch unit (Siliciclastic Flysch or Upper Aguinaga Formation) and 15 to the lower unit (Calcareous Flysch or Lower Itziar Formation).

Mineralogical and petrographic properties were analyzed by performing thin sections and studying them under a polarizing petrographic microscope in order to determine grain size and quantitative mineral content.

Geomechanical stations identified the intact rock lithology and the existing discontinuities, registering their typology (e.g. joints, faults, etc.), orientations and main properties (e.g. spacing, persistence and aperture). The rock mass fracturing state was studied by plotting the discontinuities through stereographic projection, a kind of azimuthal projection where the source point for the projection is located on the top of a sphere and the plane of projection is the equatorial plane (the hemisphere plotted corresponds to the lower one). Discontinuities were then grouped into sets of similar characteristics (typology, orientation and properties).

Boreholes were carried out by core drilling with a diameter of 89 mm. The depths investigated ranged between 16 m and 114 m and a total of 124 undisturbed rock samples were extracted in order to carry out different laboratory tests. Mechanical properties were explored by means of 90 uniaxial compressive strength tests, 18 point load tests, 25 Brazilian tests (tensile strength tests) and 12 triaxial tests (confined compression on rocks). Additionally, 12 direct shear tests were performed to obtain the angle of friction of the joints. Identification tests (e.g. unit weight) were also conducted. All of these tests were based on ISRM (2007) recommendations and ASTM standards (ASTM D7012; ASTM D3967; ASTM D5731; ASTM D2664; ASTM D5607). The value of the *RQD* (Rock Quality Design) was directly obtained from the boreholes performed (i.e. by drilling) when that was possible. Otherwise, *RQD* was obtained using the correlation given by Palmström (1974) from the volumetric joint count value J_v obtained from the geomechanical stations.

In addition, a slope inventory was carried out to assess the situation in the existing slopes in the area. A total of 44 slopes were analyzed (see **Table 1** and **Fig. 2**), identifying their geographical and geological situation, specific location, orientation, height, length, inclination and main geological, hydrogeological and geotechnical properties (including lithology, presence of water, fracture density, joint roughness, weathering and block shape). Any observed instability, such as planar failures, wedge failures, toppling, or falls due to differential erosion and earthflows, were also recorded, as well as the presence of any vegetation and erosive problems (e.g. scours, gullies, debris and differential erosion).

3.2. Geomechanical characterization

The Basic Rock Mass Rating (RMR_B) quality index was computed following the definitions in Bieniaswki (1989) for each rock mass analyzed. The index takes into account the uniaxial compressive strength of the intact rock (σ_{ci}), the *RQD*, the spacing of the discontinuities, the general features of the discontinuities (e.g. aperture, roughness and persistence) and the hydrogeological conditions of the rock mass.

The Hoek-Brown failure criterion (Hoek et al. 2002) was used to characterize the mechanical behaviour of the flysch materials. This is a failure criterion defined by the expression:

$$\sigma'_1 = \sigma'_3 + \sigma_{ci} \cdot \left(m_b \cdot \frac{\sigma'_3}{\sigma_{ci}} + s \right)^a \quad (1)$$

where σ'_1 and σ'_3 are the effective major principal stress and the effective minor principal stress, respectively and m_b, s and a are three parameters related to the intact rock type and the Geological Strength Index (*GSI*):

$$m_b = m_i \cdot \exp\left(\frac{GSI - 100}{28 - 14 \cdot D} \right) \quad (2)$$

$$s = \exp\left(\frac{GSI - 100}{9 - 3 \cdot D} \right) \quad (3)$$

$$a = \frac{1}{2} + \frac{1}{6} \cdot \left[\exp\left(-\frac{GSI}{15} \right) - \exp\left(-\frac{20}{3} \right) \right] \quad (4)$$

m_i being a constant that depends on the nature of the intact rock and D is a parameter that depends on the degree of disturbance of the rock mass. Values for the *GSI* and m_i were adopted based on the method proposed by Hoek (2000) and according to the adaptation for heterogeneous rock masses (flysch) developed by Marinos and Hoek (2001) and Marinos (2019). Disturbance factor D was considered according to the method given by Hoek et al. (2002).

4. Results

4.1. Mineralogical and petrographic properties

The Calcareous Flysch (Itziar Formation: Cenomanian-Santonian (Mathey 1982)) consists of up to 200 m of calcareous turbidites dominated by dark grey to black marls and marly limestones, rhythmically interbedded with argillaceous marls (**Figs. 3a and 3b**). Petrologically speaking, the carbonate-rich facies are micritic limestones (Folk 1962) with detritic quartz grains and dolomitic patches, or partially silicified, dolomitised wackestones according to Dunham (1962). The more siliciclastic intervals of the sequence are marls or marly limestones with abundant microfossils. Occasional thin intercalations of terrigenous sediments (quartz wackes, Pettijohn et al. 1987) are also present.

The Siliciclastic Flysch (Aguinaga Formation: Campanian-Lower Maastrichtian; Mathey 1982) consists of a thick, quartz-rich turbidite sequence overlaying the preceding calcareous turbidite formation (Eve 1988). This unit is composed of up to 500 m of interbedded, fine-grained sandy limestones, marls and sandstones, arranged in centimetric to decimetric layers, with the sandstones being the dominant lithologies (**Figs. 3c and 3d**). The thickness of the sequence is variable and there is a noticeable thickness reduction from West to East, changing from 500 m in the vicinity of Renteria to less than 250 m surrounding Hernani. The sequence was dated as Upper Santonian-Campanian (Mathey 1982; Ábalos 2016). These facies exhibit numerous water escape sedimentary structures (convolute bedding, dish and flame structures, etc.) together with abundant trace fossils (e.g. *zoophycus, paleodyction*, *chondrites*, *helmintoides*, *thalassinoides, granularia*, etc.). The fine-grained components of the succession are classified as quartz arenites (Pettijohn et al. 1987) or calcarenites (Folk 1974). The carbonate facies consist of partly-silicified, calcareous mudstones with quartz grains (Dunham 1962). These materials represent a distal turbidity fan and submarine plain deposits, formed by deep water gravity flows (Bouma sequence intervals T_c, T_d and T_e). Palaeocurrent direction analysis indicates that turbidity flows came predominantly from the North East (EVE 1998). The presence of thick mega-turbidite deposits containing blocks more than 5 m in size towards the end of the series, suggests that some sort of catastrophic event occurred.

4.2. Laboratory tests

The results obtained from laboratory identification and mechanical testing (unit weight, uniaxial compressive strength, tensile strength, point load, confined compression and shear strength of the joints) on flysch materials are summarized in **Table 2**. Siliciclastic Flysch materials showed an average dry density of 26.4 kN/m^3, a uniaxial compressive strength average value of 24.83 MPa and a tensile strength average value of 8.43 MPa. Triaxial test (confined compression) yielded average values of 10 MPa and 39.5º for cohesion and friction angle of the intact rock, respectively. In this formation, average residual friction angle of joints was found to be 23º. Calcareous Flysch materials showed an average dry density of 26.4 kN/m^3, a uniaxial compressive strength average value of 22.89 MPa and a tensile strength average value of 6.49 MPa. Triaxial test (confined compression) yielded average values of 8.6 MPa and 49º for cohesion and friction angle of the intact rock, respectively. In this formation, average residual friction angle of joints was found to be 30º.

As observed, the average values for both Calcareous Flysch and Siliciclastic Flysch are rather similar in all cases, except for the angle of friction of the discontinuities and the results of the confined compression tests, both of which showed higher mechanical values for the Calcareous Flysch materials.

4.3. Geomechanical characterization

Geomechanical stations conducted on flysch materials showed that these materials were characterized by at least 3 sets of discontinuities (occasionally 4 sets were identified). **Fig. 4a** shows an example of a geomechanical station for a material belonging to the Calcareous Flysch, while **Fig. 4b** shows one for a material belonging to the Siliciclastic Flysch. In both units, no fault was recorded. This number of sets lead to classifying the degree of fracturing of the studied rock masses as being class VI (“three sets of discontinuities”) and VII (“three sets of discontinuities plus another occasional one”) according to ISRM (1981). Moreover the block shape reported in the slope inventory indicated that the rock masses analyzed consist of tabular-prismatic blocks, vertically flattened and even sometimes exhibiting a planar shape (morphology which is expected for a flysch deposit). **Fig. 5** shows some of the slopes investigated.

Geomechanical characterization results obtained for the 33 flysch locations investigated are shown in **Table 3**. Values of uniaxial compressive strength for the intact rock (σ_{ci}), the *RQD*, the Basic Rock Mass Rating (RMR_B) quality index, the *GSI* index and the Hoek-Brown failure criterion parameters m_i, m_b, s and a (Hoek et al. 2002) are given. In addition, the mechanical properties of the flysch rock masses, i.e. uniaxial compressive strength of the rock mass (σ_c), tensile strength of the rock mass (σ_{tm}), rock mass strength (σ'_{cm}) and Young modulus of the rock mass (E_m), are also listed. The latter properties were obtained based on the expression given in Hoek and Brown (1997) and Hoek et al. (2002), as well as taking into account the modifications of Marinos and Hoek (2001):

$$\sigma_c = \sigma_{ci} \cdot s^a \tag{5}$$

$$\sigma_{tm} = -\frac{s \cdot \sigma_{ci}}{m_b} \tag{6}$$

$$\sigma'_{cm} = \frac{\sigma_{ci} \cdot \left[m_b + 4 \cdot s - a \cdot \left(m_b - 8 \cdot s \right) \right] \cdot \left(\dfrac{m_b}{4+s} \right)^{a-1}}{2 \cdot \left(1+a\right) \cdot \left(2+a\right)} \tag{7}$$

$$E_m = \left(1 - \frac{D}{2}\right) \cdot \left(\frac{\sigma_{ci}}{100}\right)^{1/2} \cdot 10^{\frac{GSI-10}{40}} \tag{8}$$

5. Analysis and Discussion

5.1. GSI vs uniaxial compressive strength

The 33 flysch materials identified in this study were plotted in a chart of *GSI* vs uniaxial compressive strength of the intact rock (σ_{ci}), following the classification approach for flysch materials developed by Morales et al. (2004) for alpine rock masses belonging to the Basque Arc. According to that classification, 8 groups are defined depending on the position of the *GSI* vs σ_{ci} pairs, ranging from very competent rock masses (massive or thick-bedded) to weak rock masses with intense jointing or low intact rock strength. **Table 4** lists the description of each rock mass class given by Morales et al. (2004) as well as the “average” values of the Hoek-Brown failure criterion (Hoek et al. 2002) parameters m_b, s and a which were also proposed by Morales et al. (2004) for each rock mass class.

Fig. 6 displays the classification chart along with the location plotted by each of the 33 investigated flysch materials. As can be seen, Siliciclastic Flysch materials (the upper flysch unit) tend to be located at regions belonging to rock mass classes 1 and 2, which correspond to competent rock masses (limestones and sandstones) with a thick-bedded, blocky structure. These materials are expected to allow steep slopes without many instability issues. This was observed to be the case in the slope inventory, where slopes of more than 25 m in height and reaching an inclination of 70º to 75º were reported to be reasonably stable, with only some retaining measures such as mesh and horizontal or vertical drains (the majority of the horizontal ones being blinded).

Conversely, Calcareous Flysch materials (lower flysch unit) do not present a clear location on the Morales et al. (2004) chart, with points in nearly all classes (except 6 and 7). However, most of them belong to rock mass class 8, i.e. to the "worst" rock mass class. This phenomenon may be put down to the existence of soft and evolutive materials (marls) in these flysch materials. Thus, where marl content is lower, rock masses tend to belong to classes 1 to 3, while the greater the content in marl, the lower the rock mass quality, up to rock mass class 8. The worse mechanical behavior of those materials was also observed in the slope inventory that was conducted, generally finding that, in general, they formed slopes of reduced height (around 3 to 4 m) and with inclinations of about 45º.

It should be mentioned that marls were not present in the Siliciclastic Flysch materials, so the mechanical behavior of those rock masses is mainly given by their discontinuities. This results in better geomechanical characteristics and higher values (**Table 5**) of the rock mass parameters (e.g. σ_c, σ_{tm}, σ'_{cm} and E_m), all of which translates into belonging to rock mass classes 1 and 2.

5.2. GSI vs. RMR correlation

Morales et al. (2004) also proposed a correlation between the Basic Rock Mass Rating (RMR_B) quality index and the Geological Strength Index (GSI). The correlation is:

$$GSI = 4.714 + 0687 \cdot RMR_B \tag{9}$$

Fig. 7 tests the suitability of a such relationship on the 33 locations under study by comparing the *GSI* obtained directly from observation of the geological formations, as indicated by Hoek (2000) and Marinos and Hoek (2001), with the *GSI* obtained after applying the aforementioned correlation from the computed RMR_B. As observed, a high value of the coefficient of determination is obtained ($R^2 > 90\%$), so the correlation of Eq. (9) may be used for estimating the *GSI* of the flysch materials of the area under study from the RMR_B values with a good confidence level.

It is interesting to note that, even though materials studied by Morales et al. (2004) and those assessed in the present paper both come from the same geographical/geological region (the Basque Arc), the other authors did not analyze any samples from the area where the 33 studied samples were obtained (see Section 1). Thus, the good match between the proposed rock mass classification and the observed slope status in the slope inventory, as well as the high R^2 value found in the *GSI* vs. RMR_B correlation, confirms the appropriateness of the work of Morales et al. (2004) for characterizing flysch formations.

5.3. Rock mass mechanical parameters

Since Morales et al. (2004) proposed representative values of the Hoek-Brown failure criterion parameters (Hoek and Brown 1997; Hoek et al. 2002; Marinos and Hoek 2001) for rock masses belonging to each defined class, the usefulness of that classification to estimate the shear strength of flysch rock masses may be evaluated. As indicated by Hoek et al. (2002), equivalent cohesion (*c*) and friction angle (ϕ) for a rock mass can be directly obtained from:

$$c = \frac{\sigma_{ci} \cdot \left[(1+2\cdot a)\cdot s + (1-a)\cdot m_b \cdot \sigma'_{3n}\right] \cdot \left(s + m_b \cdot \sigma'_{3n}\right)^{a-1}}{(1+a)\cdot(2+a)\cdot\sqrt{\dfrac{1+\left[6\cdot a \cdot m_b \cdot \left(s+m_b\cdot\sigma'_{3n}\right)^{a-1}\right]}{(1+a)\cdot(2+a)}}} \tag{10}$$

$$\phi = \arcsin\left[\frac{6\cdot a\cdot m_b \cdot \left(s+m_b\cdot\sigma'_{3n}\right)^{a-1}}{2\cdot(1+a)\cdot(2+a) + 6\cdot a\cdot m_b\cdot\left(s+m_b\cdot\sigma'_{3n}\right)^{a-1}}\right] \tag{11}$$

where m_b, *s* and *a* are the three parameters that define the Hoek-Brown failure criterion and:

$$\sigma'_{3n} = \sigma'_{3\max} / \sigma_{ci} \quad (12)$$

σ'_{3max} being the upper limit of confining stress.

Fig. 8 shows the comparison between the strength parameters (cohesion and friction angle) obtained using Eq. (10) and Eq. (11) for the 33 flysch locations studied using the Hoek-Brown failure criterion parameters m_b, s and a (which were found experimentally, as indicated in **Table 3**) and the ones given directly by the Morales et al. (2004) classification, according to the rock mass class to which each location analyzed belongs (**Table 4**). For both calculations, the value of the upper limit of confining stress (σ'_{3max}) was taken to be equal to $0.25 \cdot \sigma_{ci}$ (Morales et al. 2004).

Together with that assessment, the graphs also show a comparison between the strength parameters obtained from experimental values and those obtained by the classical correlation of Bieniawski (1979):

$$c = 5 \cdot RMR \quad (13)$$

$$\phi = \frac{RMR}{2} + 5^{\circ} \quad (14)$$

where the RMR was taken to be equal to the RMR_B computed for each of the 33 flysch locations studied.

The results indicate a good coefficient of determination (R^2 = 86%) when estimating the value of cohesion (c) from the Hoek-Brown failure criterion parameters m_b, s and a given by the rock mass classification of Morales et al. (2004). Correlation is much lower (R^2 = 59%) when estimating the value using the Bieniawski (1979) correlation, by means of the *RMR*. The better performance of the rock mass classification from Morales et al. (2004) confirms the good degree of appropriateness of that classification for analyzing flysch formations. The poor results for *RMR* may be explained by the fact that, even though it is universally used in all rock masses in general, the *RMR* index was originally developed for igneous rocks (especially for granitic rock masses), which tend to present prismatic block shapes, while flysch formations are normally characterized by tabular and planar block shapes.

Regarding the friction angle ϕ, both the *RMR* and the use of Morales et al. (2004) classification values produce a low coefficient of determination with lower statistical significance (R^2 approximately 60%). In the case of the *RMR*, this bad performance may have its roots in the same reasons as those indicated above for the cohesion value. In terms of the Morales et al. (2004) classification, poor performance may be attributed to the wide graphical area to which each rock mass class is related in the *GSI* vs. σ_{ci} chart (**Fig. 6**). Besides, of the two parameters involved, the *GSI* appears to have more importance in the classification. For instance, all rock masses with a *GSI* of more than 50 belong to rock mass class 1, regardless of the value of the intact rock strength. Similar issues may be observed with the other classes. Thus, use of the Morales et al. (2004) classification may give a good estimation of the cohesion (whose relationship with the *GSI* is probably higher in a rock mass than with the uniaxial compressive strength of the intact rock), but only produces a rough estimation of the friction angle.

Finally, **Fig. 9** shows the performance of the *RMR* in estimating the Young modulus (E_m) of the rock mass. Two correlations were used in this analysis. The one proposed by Read et al. (1999):

$$E_m = 0.1 \cdot \left(\frac{RMR}{10} \right)^{10} \qquad (15)$$

And that proposed by Gokceoglu et al. (2003):

$$E_m = 0.0736 \cdot e^{0.0755 \cdot RMR} \qquad (16)$$

These correlations were applied to the 33 flysch locations studied and compared with the values of E_m obtained using Eq. (8) following the Hoek-Brown failure criterion (Hoek and Brown 1997; Hoek et al. 2002; Marinos and Hoek 2001). As can be seen, the Read et al. (1999) correlation is capable of capturing E_m values appropriately (R^2 near 80%), but performance is even higher (R^2 > 90%) when using the correlation of Gokceoglu et al. (2003). Thus, these correlations may be used to estimate the rock mass Young modulus of flysch formations. It is important to mention that other classical proposals like those of Bieniawski (1973) and Serafim and Pereira (1983) were also tested but their significance was very low (values of R^2 obtained were lower than 50%), so they are not appropriate for such estimations.

7. Conclusion

A geomechanical characterisation of the flysch materials in an area of about 100 km^2 in the North East of Spain was conducted. A total of 33 locations were analyzed through a complete geotechnical investigation involving boreholes, geomechanical stations, a slope inventory and laboratory tests. The materials studied corresponded to the "Upper Cretaceous Flysch"; two formations were distinguished: the Lower, "Calcareous Flysch", and the Upper, "Siliciclastic Flysch". From the different analyses performed, the following conclusions may be drawn:

- The use of the *GSI* vs. uniaxial compressive strength of the intact rock (σ_{ci}) chart given by Morales et al. (2004) is appropriate for characterizing the flysch material.
- Siliciclastic Flysch materials (upper flysch unit) are mainly rock mass classes 1 and 2 according to Morales et al. (2004) and showed good geomechanical characteristics. On the other hand, Calcareous Flysch materials (lower flysch unit) showed poor geomechanical characteristics and do not present a clear location in the Morales et al. (2004) chart but, due to the existence of soft and evolutive materials (marls) in this flysch unit, many of the samples studied correspond to the "worst" rock mass class (rock mass class 8).
- Estimation of shear strength parameters (cohesion and friction angle) for Upper Cretaceous Flysch materials was poor. Neither the estimations using the RMR index nor the ones using the Hoek-Brown failure criterion parameters (m_b, s and a) given by Morales et al. (2004) yielded a good performance, especially in terms of the friction angle. Further investigation is therefore needed in this field.

Acknowledgements

This research did not receive any specific grant from funding agencies in the public, commercial, or not-for-profit sectors. Authors thank to Spanish companies PROYEX, S.A. and IBERGEOTECNIA, S.R.L. as well as to the geologist M. Estefanía Bona for providing the geotechnical data. The authors fully acknowledge the financial support provided by the Department of Geological and Geotechnical Engineering of the UPV. The original version of the manuscript was submitted for professional proofreading.

References

Ábalos B (2016) Geologic Map of the Basque Cantabrian Basin and a new tectonic interpretation of the Basque Arc. International Journal of Earth Sciences (Geologische Rundschau) 105:2327–2354.

Ábalos B, Alkorta A, Iríbar V (2008) Geological and isotopic constraints on the structure of the Bilbao anticlinorium (Basque-Cantabrian basin, North Spain). Journal of Structural Geology 30:1354–1367.

Akin M (2013) Slope Stability Problems and Back Analysis in Heavily Jointed Rock Mass: A Case Study from Manisa, Turkey. Rock Mech Rock Eng 46:359–371.

ASTM D2664 (2004) Standard Test Method for Triaxial Compressive Strength of Undrained Rock Core Specimens Without Pore Pressure Measurements. American Society for Testing and Materials, West Conshohocken, PA.

ASTM D3967 (2001) Standard test method for splitting tensile strength of intact rock core specimens. American Society for Testing and Materials, West Conshohocken, PA.

ASTM D5607 (2016) Standard Test Method for Performing Laboratory Direct Shear Strength Tests of Rock Specimens Under Constant Normal Force. American Society for Testing and Materials, West Conshohocken, PA.

ASTM D5731 (2007) Standard Test Method for Determination of the Point Load Strength Index of Rock and Application to Rock Strength Classifications. American Society for Testing and Materials, West Conshohocken, PA.

ASTM D7012 (2010) Standard test method for compressive strength and elastic module of intact rock core specimens under varying states of stress and temperatures. American Society for Testing and Materials, West Conshohocken, PA.

Baceta JA, Orue-Etxebarria X, Apellaniz E (2011) El flysch entre Deba y Zumaia/ The flysch between Deba and Zumaia. Enseñanza de las Ciencias de la Tierra 18(3):269-283.

Barton N, Lien R, Lunde J (1974) Engineering classification of rock masses for the design of tunnel support. Rock Mechanics 6(4):189–236.

Bieniawski ZT (1973) Engineering classification of jointed rock masses. South African Institution of Civil Engineering 15(12):335–344.

Bieniawski ZT (1979) The geomechanics classification in rock engineering applications. 4th International Conference on Rock Mechanics, Montreaux, Switzerland.

Bieniawski ZT (1989) Engineering rock mass classifications. John Wiley and Sons, Inc.

Bouma AH (1962). Sedimentology of some Flysch Deposits. A Graphic Aproach to Facies Interpretation. Elsevier, Amsterdam, 168 pp.

Cámara P (1997) The Basque-Cantabrian Basin's Mesozoic tectonosedimentary evolution. Mémoire de la Société Géologique de France 171:167–176

Cano M, Tomás R (2013) Characterization of the instability mechanisms affecting slopes on carbonatic Flysch: Alicante (SE Spain), case study. Eng Geol 156:68–91.

Saroglou C, Qi S, Guo S, Wu F (2019) ARMR, a new classification system for the rating of anisotropic rock masse. Bulletin of Engineering Geology and the Environment 78:3611–3626.

Dunham RJ (1962) Classification of carbonate rocks according to depositional texture. In: Ham, WE (ed) Classification of carbonate rocks: A symposium. American Association of Petroleum Geologists, Memoir 1, 108–121.

EVE (1998) Geological map of Basque Country, scale 1:25.000. Sheet no. 64-II, San Sebastian. Ente Vasco de Energía, 54 pp [in Spanish].

Feuillée P, Rat P (1971) Structures et paléogéographies pyrénéocantabriques. In: Debyser J, Le Pichon X, Montadert L (eds) Histoire Structurale du Golfe de Gascogne. Publications de l'Institut Français du Pétrole, Collection Colloques et Séminaires 22(2):1–48.

Folk RL (1962) Spectral subdivisions of limestone types. In: Ham WE (ed) Classification of carbonate rocks: A symposium, American Association of Petroleum Geologists, Memoir 1, pp. 62-85.

Folk RL (1974) The Petrology of Sedimentary Rocks. Hemphill Publishing Co. Austin, Texas. 182 pp.

Fortsakis P, Nikas K, Marinos, V, Marinos P (2012) Anisotropic behaviour of stratified rock masses in tunnelling. Engineering Geology 141-142 (19):74–83.

García-Mondéjar J, Agirrezabala LM, Aranburu A, Fernández-Mendiola PA, Gómez-Pérez I, López-Horgue M, Rosales I (1996) Aptian-Albian tectonic pattern of the Basque-Cantabrian Basin (northern Spain). Geological Journal 31:13–45.

Gokceoglu C, Sonmez H, Kayabasi A (2003) Predicting the deformation moduli of rock masses. International Journal of Rock Mechanics and Mining Sciences 40(5):701-710.

Gómez M, Verges J, Riaza C (2002) Inversion tectonics of the Northern margin of the Basque Cantabrian Basin. Bulletin de la Société Géologique de France 173:449–459.

Gong M, Qi S, Liu J (2010) Engineering geological problems related to high geo-stresses at the Jinping I Hydropower Station, Southwest China. Bulletin of Engineering Geology and the Environment 69:373–380.

Hoedemaeker PhJ (1973) Olisthostromes and other delapsional deposits, and their occurrence in the region of Moratalla (Prov. Of Murcia, Spain). Scripta Geologica 19:1–197.

Hoek E (2000) Rock Engineering. Course Notes by Evert Hoek. Balkema, Rotterdam. 313 pp.

Hoek E, Brown ET (1997) Practical estimates of rock mass strength. International Journal of Rock Mechanics and Mining Sciences 34(8):1165–1186.

Hoek E, Carranza-Torres C, Corkum B (2002) Hoek-Brown failure criterion – 2002 Edition. In: Hammah R, Bawden W, Curran J, Telesnicki M (eds) Proceedings of NARMSTAC 2002, Mining Innovation and Technology, Toronto.

ISRM (1981) Suggested methods for rock characterization, testing and monitoring. International Society for Rock Mechanics. Pergamon Press, Oxford.

ISRM (2007) The Complete ISRM suggested methods for rock characterization, testing and monitoring: 1974–2006. International Society for Rock Mechanics, Lisbon.

Kuenen PhH, Migliorini CI (1950) Turbidity currents as a cause of graded bedding. J. Geol. 58:91–127.

Le Pichon X, Bonnin J, Francheteau J, Sibuet JC (1971) Une hypothèse d´évolution tectonique du golfe de Gascogne. In: Histoire structurale du Golfe de Gascogne. Editions Technip, Paris.

Marinos P (2019) A revised, geotechnical classification GSI system for tectonically disturbed heterogeneous rock masses, such as flysch. Bulletin of Engineering Geology and the Environment 78:899–912.

Marinos V, Fortsakis P, Prountzopoulos G (2006) Estimation of rock mass properties of heavily sheared flysch using data from tunnelling construction. Proceedings of the 10th IAEG International Congress, Nottingham.

Marinos V, Fortsakis P, Prountzopoulos G (2011) stimation of geotechnical properties and classification of geotechnical behaviour in tunnelling for flysch rock masses. Proceedings of the 15th European Conference on Soil Mechanics and Geotechnical Engineering, Athens, 1:435–440.

Marinos P, Hoek E (2001) Estimating the geotechnical properties of heterogeneous rock masses such as flysch. Bulletin of Engineering Geology and the Environment 60:82–92.

Mathey B (1982) El Cretácico superior del Arco Vasco. In: García A (ed) El Cretácico de España. Universidad Complutense de Madrid, Madrid, 111–135.

Mary C, Moreau M-G, Orue-Etxebarria X, Apellaniz E, Courtillot, V (1991) Biostratigraphy and magnetostratigraphy of the Cretaceous/Tertiary Sopelana section (Basque country). Earth Planetary Science Letters 106:133–150.

Morales T, Uribe-Etxebarria G, Uriarte JA, Fernández de Valderrama I (2004) Geomechanical characterisation of rock masses in Alpine regions: the Basque Arc (Basque-Cantabrian basin, Northern Spain). Engineering Geology 71:343–362.

Mutti E, Bernoulli E, Ricci Lucchi F, Tinterri R (2009) Turbidites and turbidity currents from Alpine “flysch” to the exploration of continental margins. Sedimentology 56:267–318.

Mutti E, Tinterri R, Benevelli G, DiBiase D, Cavanna G (2003) Deltaic, mixed and turbidite sedimentation of ancient foreland basins. In: Mutti E, Steffens GS, Pirmez C, Orlando M, Roberts D (eds) Turbidites: Models and Problems. Marine and Petroleum Geology 20:733–755.

Palmstrom A (1974) Characterization of jointing density and the quality of rock masses (in Norwegian). Internal report, A.B. Berdal, Norway.

Pettijohn F, Potter PE, Siever R (1987). Sand and Sandstone, 2nd ed. Springer-Verlag. 553 pp.

Popiolek S, Sala H, Thiel K (1993) Geotechnical Flysch Rock Mass Classification (KF). In: Thiel K, Zabuski I (eds) Proc. of Seminar on underground structures in complex geological conditions, Swinna Poreba, Poland. Institute of Meteorology and Water Management, Warsaw, 27–39.

Pujalte V, Baceta JI, Dinarès-Turell J, Orue-etxebarria X, Parés JM, Payros A (1995) Biostratigraphic and magnetostratigraphic intercalibration of latest Cretaceous and Paleocene depositional sequences from the deep-water Basque Basin, western Pyrenees, Spain. Earth Planetary Science Letters 136:17–30.

Pujalte V, Baceta JI, Orue-Etxebarria X, Payros A (1998) Paleocene Strata of the Basque Country, estern Pyrenees, Northern Spain: facies, and sequence development in a deep-water starved basin. In: Mesozoic and Cenozoic Sequence Stratigraphy of European Basins, SEPM Special Publication:311–328.

Read SAL, Richards LR, Perrin ND (1999). Applicability of the Hoek–Brown failure criterion to New Zealand greywacke rocks. Proceedings of the 9th International Congress on Rock Mechanics, Paris.

Roca E, Muñoz JA, Ferrer O, Ellouz N (2011) The role of the Bay of Biscay extensional structure in the configuration of the Pyrenean orogen: contraints from the MARCONI Deep Seismic Reflection survey. Tectonics 30(TC 2001):1–33.

Sanders JE (1965) Primary sedimentary structures formed by turbidity currents and related resedimentation mechanisms. In: Middleton GV (ed) Primary Sedimentary Structures and their Hydrodynamic Interpretation. SEPM Spec Publ, 12:192–219.

Serafim JL, Pereira JP (1983 Considerations of the geomechanical classification of Bieniawski. International Symposium on Geological Engineering and Underground Construction, Lisbon.

Tugend J, Manatschal G, Kuzsnir NJ, Masini E, Mohn G, Thinon I (2014) Formation and deformation of hyperextended rift systems: insights from rift domain mapping in the Bay of Biscay-Pyrenees. Tectonics 33:1239–1276.

Ünal E (1996) Modified Rock Mass Classification: M-RMR System. In: Milestones in Rock Engineering, the Bieniawski Jubilee Collection, Balkema, Rotterdam, 203-223.

Vassilis M (2019) Application of the GSI System to the Classification of Soft Rocks. In: Kanji M, He M, Ribeiro e Sousa L (eds) Soft Rock Mechanics and Engineering, Springer Nature, 503-539.

Wu LZ, Li B, Huang RQ, Sun P (2017) Experimental study and modeling of shear rheology in sandstone with non-persistent joints. Engineering Geology 222:201-211

Ziegler PA (1988) Evolution of the Arctic-North Atlantic and the Western Tethys: AAPG Memoir 43, 198 pp.

List of Figures

Fig. 1 Simplified geologic map of the eastern portion of the Basque-Cantabrian Basin showing the location of the study area (star). Inset indicates the location of the detailed map depicted in Fig. 2. Modified from Ábalos (2016).

Fig. 2. Detailed geologic map and schematic stratigraphic section of the studied area showing sample locations (33) on the "Calcareous Flysch" (blue stars) and the "Siliciclastic Flysch" (red stars). The slope inventory carried out is also displayed (red and blue circles). The dashed line represents the Hernani-Renteria railway stretch. Modified from EVE (1988).

Fig. 3. Photomicrographs of the terrigenous and carbonatic microfacies of the studied materials: (a) Siltstone of the "Calcareous Flysch"; (b) Mudstone of the "Calcareous Flysch"; (c) Quartzarenite of the "Siliciclastic Flysch". Note that the margins of some of the quartz grains arc scalloped in contact with the clays of the matrix. This has occurred as a result of corrosion of the quartz during diagenesis; (d) Mudstone in the "Siliciclastic Flysch". The micritic matrix is partly recrystallized to microspar and partly dolomitized. **Abbreviations**: **ca**, sparry calcite; **cm**, clayey matrix; **d**, dolomite; **m**, micrite; **Q**, quartz. All figures under cross-polarized light.

Fig. 4. Geomechanical stations: (a) geomechanical station on Calcareous Flysch materials; (b) geomechanical station on Siliciclastic Flysch materials. Corresponding joint sets are depicted in the pictures. For each set, its dip and dip direction is indicated.

Fig. 5. Some slopes investigated in the slope inventory: (a) and (b) "Calcareous Flysch" slopes (approximate height 3.5 m and 4 m, respectively; inclination 55º and 45º, respectively. Materials consist of thick layers of marls and marly limestones alternating with argillaceous limestones which dip downward about 25º to the SE); (c) and (d) "Siliciclastic Flysch" slopes (approximate height 8 m and 14 m, respectively; inclination 65º and 75º, respectively. The rocks are basically thin-bedded fine-grained sandy linmestones interbbeded with less competent layers of marls placed in centimetric to demimetric layers. The whole sequence dips at 45º towards the North).

Fig. 6. Location of the 33 flysch samples studied in a *GSI* vs. uniaxial compressive strength of the intact rock chart, inside the 8 rock mass classes defined by Morales *et al*. (2004).

Fig. 7. Relationship between the *GSI* experimentally obtained and the *GSI* computed from the value of the *RMR* according to the proposal of Morales *et al*. (2004).

Fig. 8. Shear strength parameters assessment: (a) Cohesion; (b) Friction angle. "Experimental data" values were based on computing Hoek-Brown failure criterion (Hoek and Brown, 1997; Hoek *et al*., 2002; Marinos and Hoek, 2001) parameters m_b, s and a experimentally obtained (listed in Table 3) and applying Hoek *et al*. (2002) expressions for cohesion and friction angle. "Estimated" values were obtained either from the Hoek-Brown failure criterion parameters m_b, s and a given by the rock mass class according to Morales *et al*. (2004) or from the RMR through Bieniawski's (1979) correlation.

Fig. 9. Comparison between the rock mass Young modulus (E_m) obtained from the *GSI* (Hoek and Brown, 1997; Hoek *et al*., 2002) and that one obtained by correlations with the *RMR*.

List of Tables

Figure 1

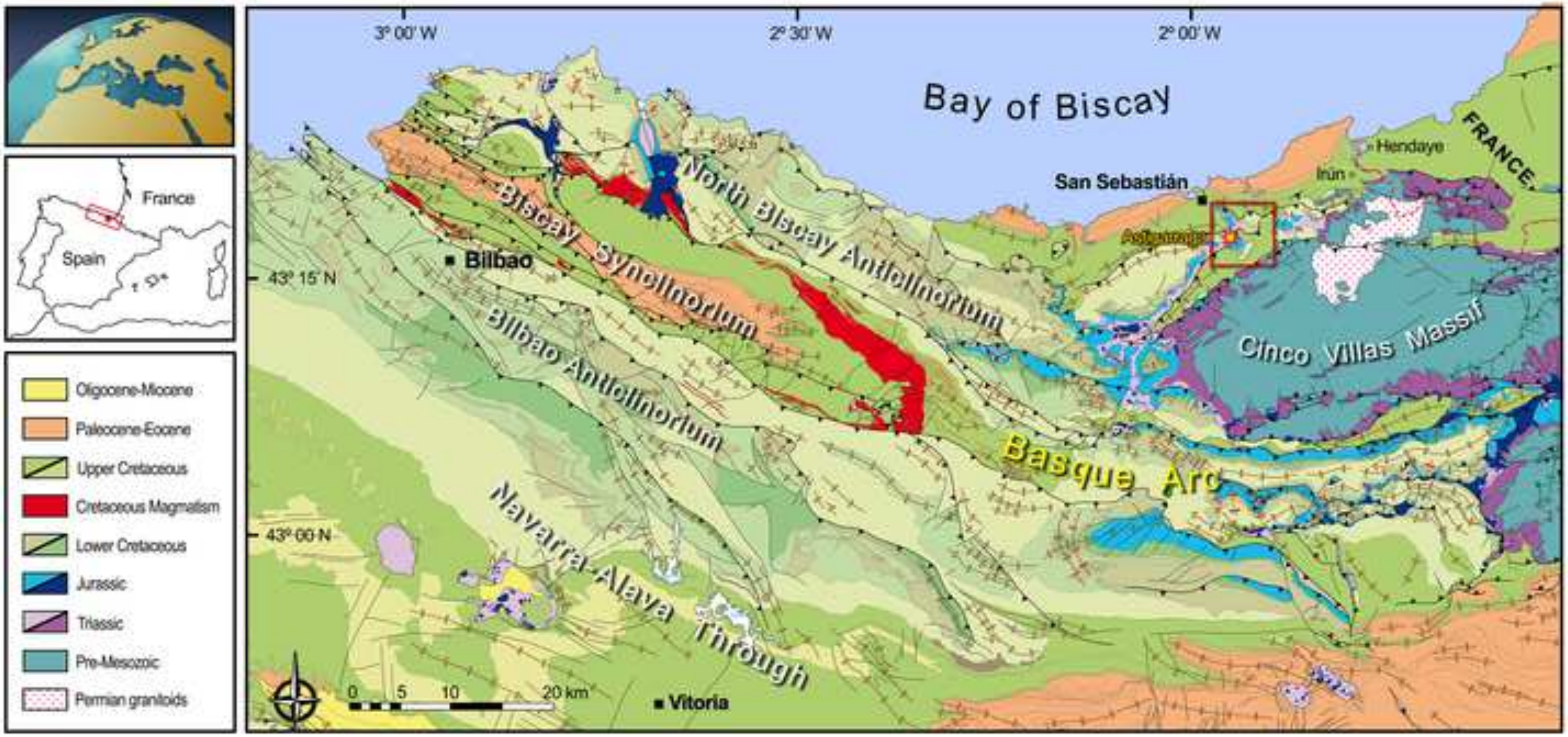

France
Spain
Oligocene-Miocene
Paleocene-Eocene
Upper Cretaceous
Cretaceous Magmatism
Lower Cretaceous
Jurassic
Triassic
Pre-Mesozoic
Permian granitoids
3° 00' W
2° 30' W
2° 00' W
43° 15' N
43° 00' N
Bay of Biscay
FRANCE
Hendaye
Irún
San Sebastián
Bilbao
Vitoria
Biscay Synclinorium
North Biscay Anticlinorium
Bilbao Anticlinorium
Cinco Villas Massif
Basque Arc
Navarra-Alava Through
0
5
10
20 km

Figure 2

Click here to access/download;Figure;Figure 2 (500dpi_full page width).jpg

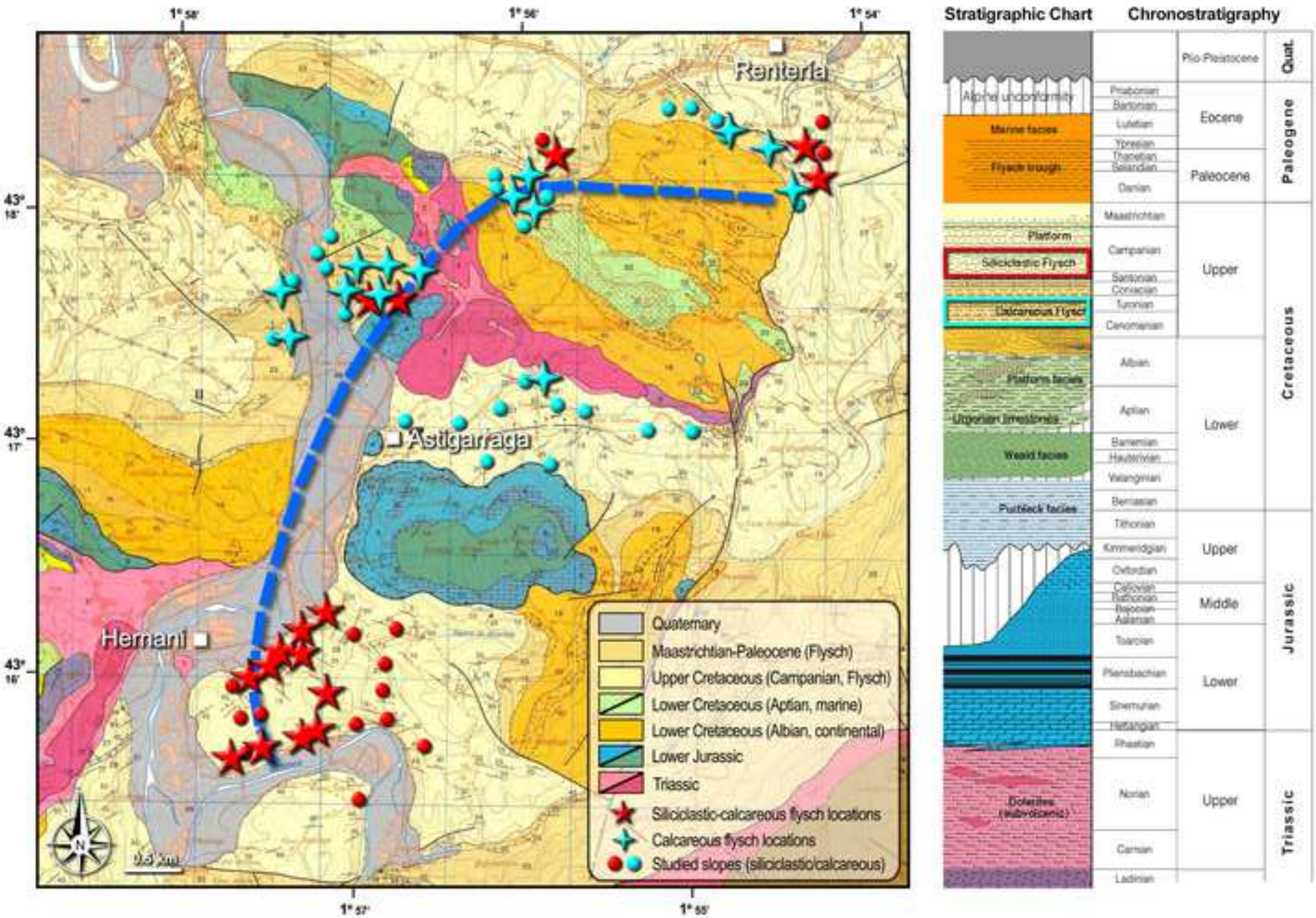

Figure 3

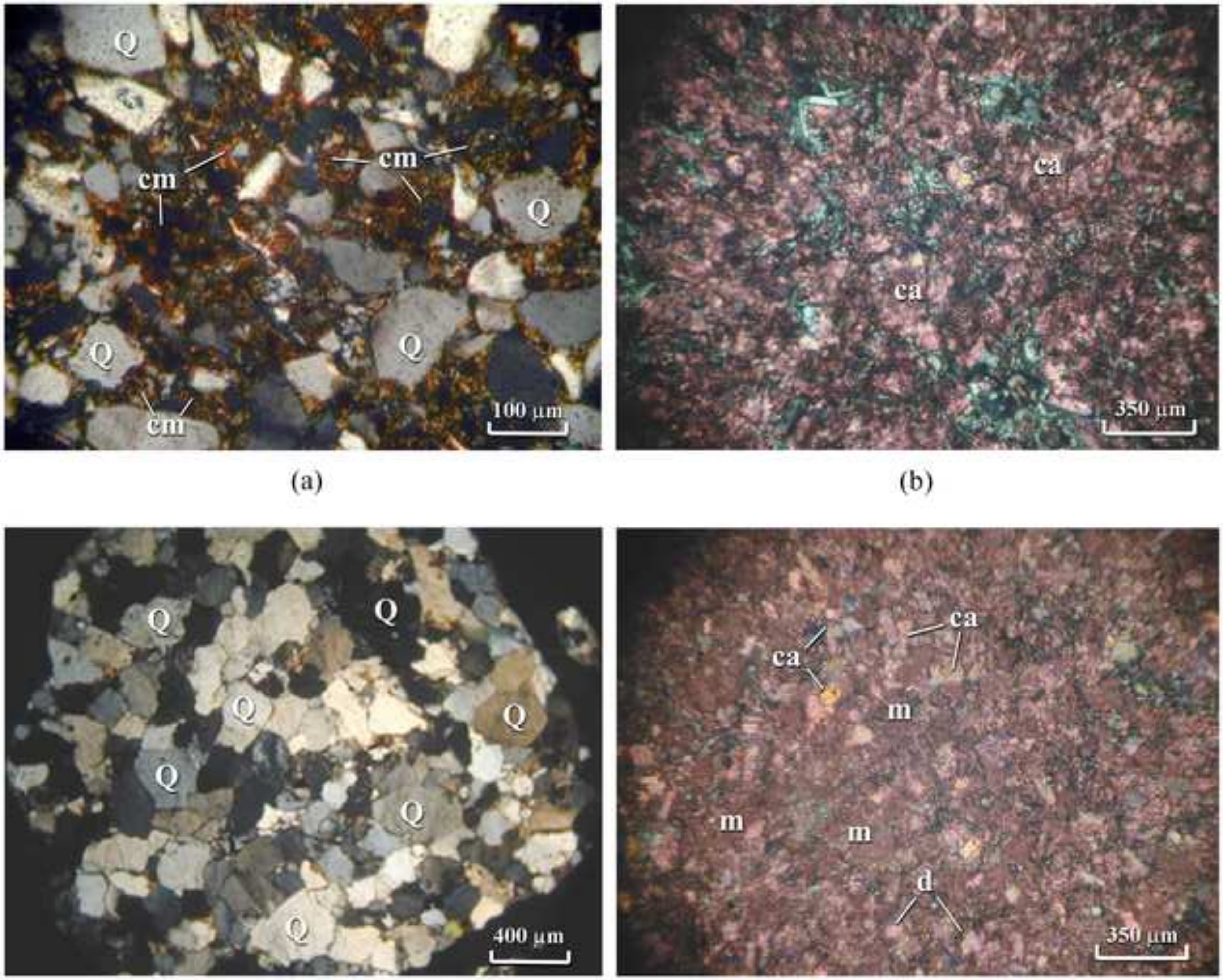

(a) (b) (c) (d)

Figure 4

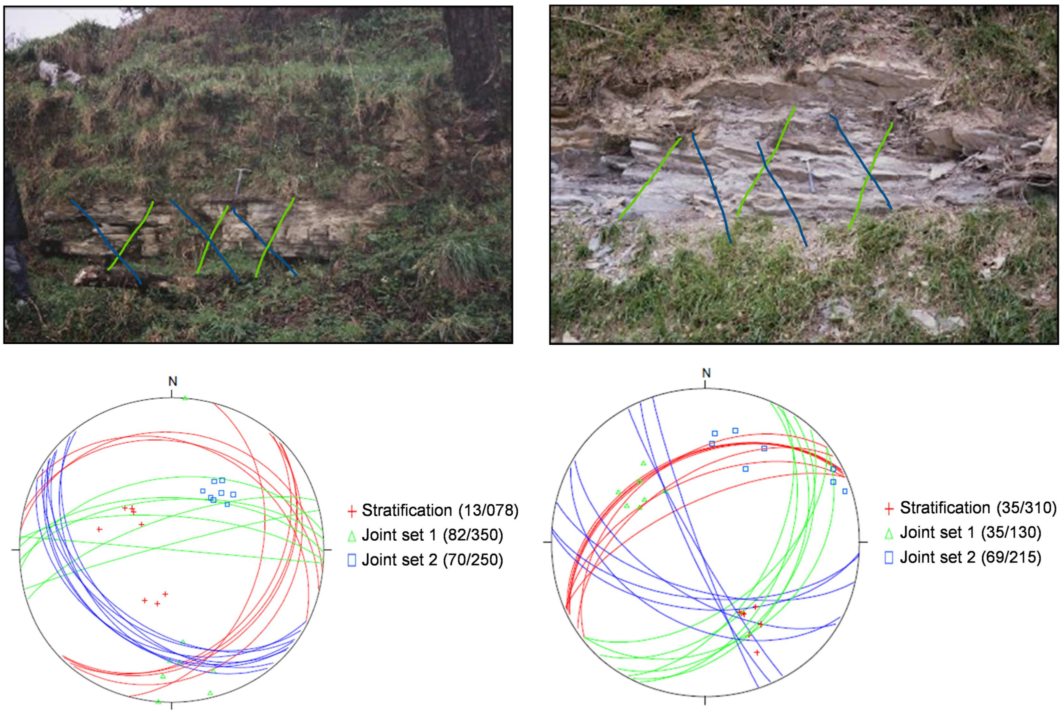
N
Stratification (13/078)
Joint set 1 (82/350)
Joint set 2 (70/250)
N
Stratification (35/310)
Joint set 1 (35/130)
Joint set 2 (69/215)

(a) (b)

Figure 5

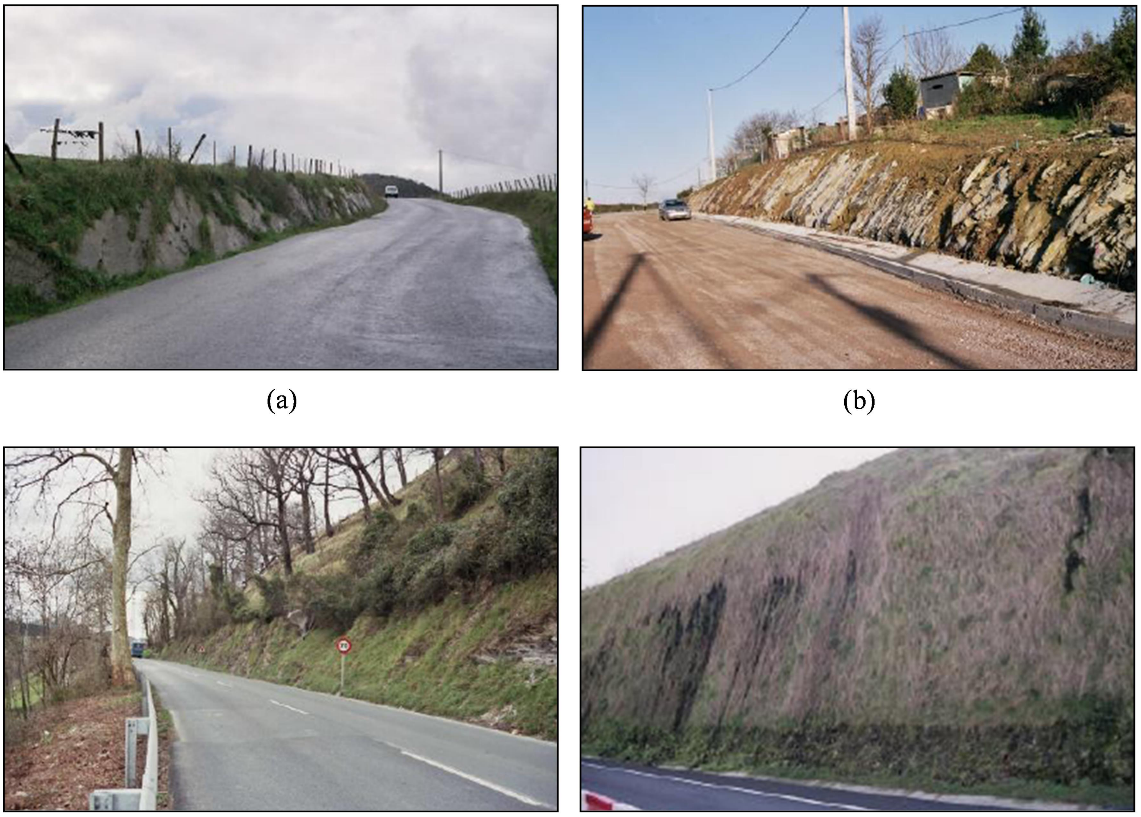

(a) (b)

(c) (d)

Figure 6

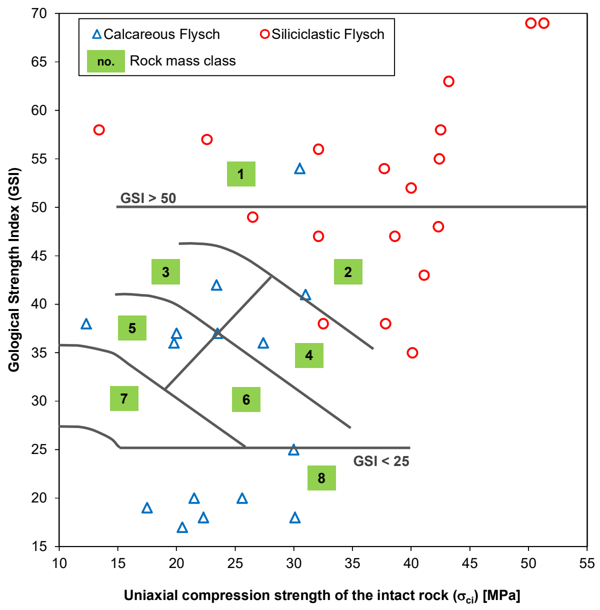

Calcareous Flysch
Siliciclastic Flysch
no.
Rock mass class
GSI > 50
GSI < 25
1
2
3
4
5
6
7
8
Gological Strength Index (GSI)
Uniaxial compression strength of the intact rock (σ_{ci}) [MPa]

Figure 7

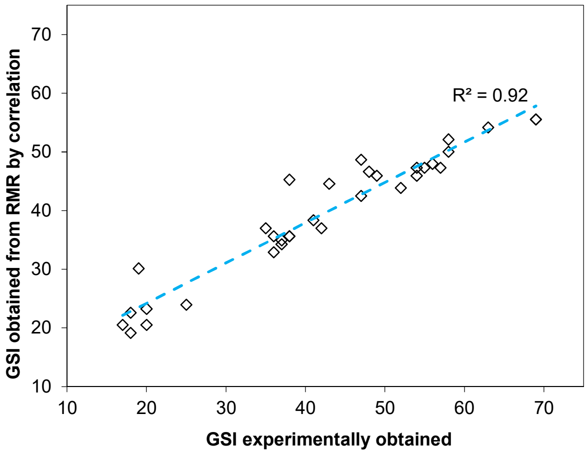
R² = 0.92
GSI obtained from RMR by correlation
GSI experimentally obtained
10
20
30
40
50
60
70
10
20
30
40
50
60
70

Figure 8

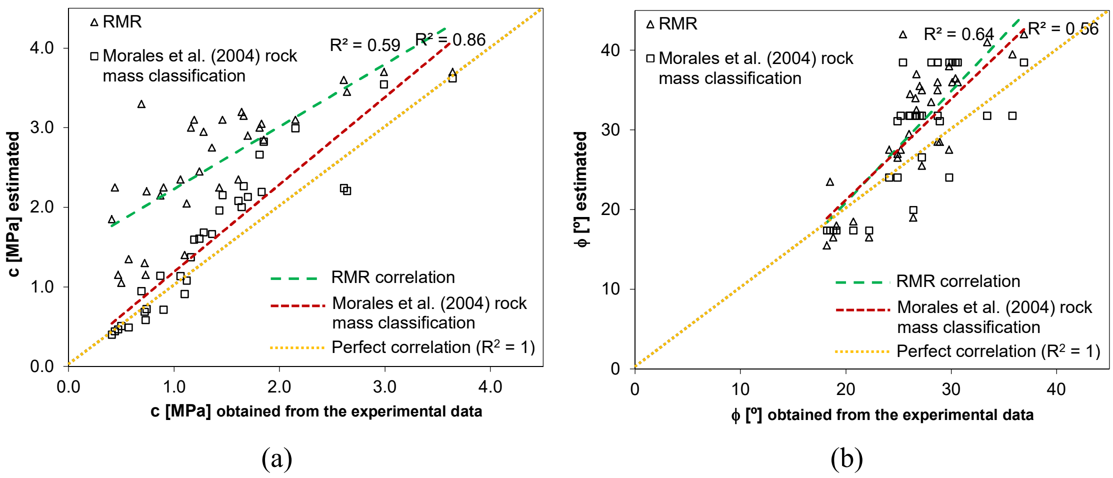
RMR
Morales et al. (2004) rock mass classification
R² = 0.59
R² = 0.86
c [MPa] estimated
c [MPa] obtained from the experimental data
RMR correlation
Morales et al. (2004) rock mass classification
Perfect correlation (R² = 1)
0.0
1.0
2.0
3.0
4.0
(a)
RMR
Morales et al. (2004) rock mass classification
R² = 0.64
R² = 0.56
ϕ [º] estimated
ϕ [º] obtained from the experimental data
RMR correlation
Morales et al. (2004) rock mass classification
Perfect correlation (R² = 1)
0
10
20
30
40
(b)

Figure 9

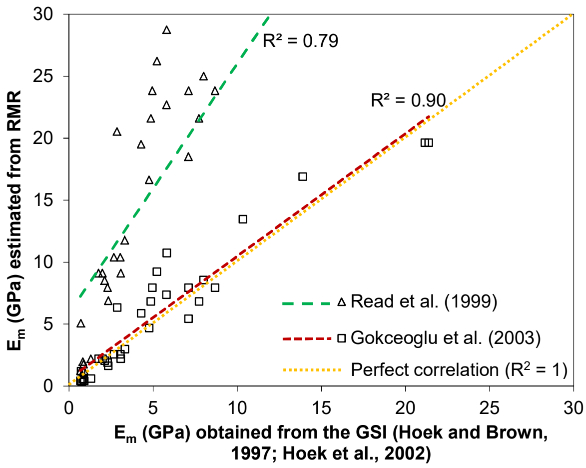

30
25
20
15
10
5
0
0
5
10
15
20
25
30
R² = 0.79
R² = 0.90
Read et al. (1999)
Gokceoglu et al. (2003)
Perfect correlation (R² = 1)
Em (GPa) estimated from RMR
Em (GPa) obtained from the GSI (Hoek and Brown, 1997; Hoek et al., 2002)

Table 1

Table 1. Basic data of the slope inventory.

Slope	Lithology	Geologic unit	Height (m)	Tilt / Geometry
S-1	Marly limestones	Calcareous flysch	8	1H/2V
S-2	Marly limestones	Calcareous flysch	3	2H/3V
S-3	Siliceous sandstones	Siliciclastic flysch	2’5	Subvertical
S-4	Siliceous sandstones	Siliciclastic flysch	6	1H/3V
S-5	Calcareous marls	Calcareous flysch	4	2H/3V
S-6	Limestones	Calcareous flysch	30	1H/2V
S-7	Limestones	Calcareous flysch	30	Subvertical
S-8	Limestones	Calcareous flysch	30	Subvertical
S-9	Marly limestones	Calcareous flysch	5	1H/3V
S-10	Marly limestones	Calcareous flysch	5	1H/3V
S-11	Marly limestones	Calcareous flysch	1’5	2H/3V
S-12	Siliceous sandstones	Siliciclastic flysch	8-9	Subvertical
S-13	Siliceous sandstones	Siliciclastic flysch	10	Subvertical
S-14	Grey limestones	Calcareous flysch	15	2H/3V
S-15	Grey-blue marls	Calcareous flysch	8	1H/1V
S-16	Sandstones and siltstones	Siliciclastic flysch	12	1H/3V
S-17	Grey marls	Calcareous flysch	5	1H/3V
S-18	Grey marls	Calcareous flysch	10	1H/3V
S-19	Limestones	Calcareous flysch	3	Subvertical
S-20	Marly limestones	Calcareous flysch	10	1H/3V
S-21	Sandstones and siltstones	Siliciclastic flysch	7	Subvertical
S-22	Sandstones and siltstones	Siliciclastic flysch	3	1H/4V
S-23	Sandstones and siltstones	Siliciclastic flysch	15	1H/4V
S-24	Grey limestones	Calcareous flysch	10	Subvertical
S-25	Grey limestones	Calcareous flysch	20	1H/3V
S-26	Laminated marls	Calcareous flysch	3’5	2H/3V
S-27	Calcareous marls	Calcareous flysch	3	2H/3V
S-28	Siliceous microconglomerates	Siliciclastic flysch	7	1H/3V
S-29	Limestones	Calcareous flysch	6	Subvertical
S-30	Siliceous sandstones	Siliciclastic flysch	6	Subvertical
S-31	Siliceous sandstones	Siliciclastic flysch	3’5	1H/4V
S-32	Siliceous sandstones	Siliciclastic flysch	7-8	1H/3V
S-33	Sandstones	Siliciclastic flysch	25	3H/2V
S-34	Siliceous microconglomerates	Siliciclastic flysch	3’5	Subvertical
S-35	Siliceous sandstones	Siliciclastic flysch	9	Subvertical
S-36	Sandstones and conglomerates	Siliciclastic flysch	10	Subvertical
S-37	Calcareous marls	Calcareous flysch	5	1H/2V
S-38	Calcareous marls	Calcareous flysch	12	1H/1V
S-39	Laminated marls	Calcareous flysch	4	1H/1V
S-40	Limestones	Calcareous flysch	14	1H/3V
S-41	Calcareous marls	Calcareous flysch	14	1H/1V
S-42	Calcareous marls	Calcareous flysch	25	2H/3V
S-43	Calcareous marls	Calcareous flysch	18	1H/1V
S-44	Calcareous marls	Calcareous flysch	21	2H/3V

Table 2

Table 2. Laboratory tests results on flysch units.

Geological unit		Unit weight (dry), γ_d (kN/m^3)	Uniaxial compression strength (MPa)	Tensile strength (MPa)	Point load, I_{s50} (MPa)	Triaxial test on rocks (confined compression)		Shear strength of joints, ϕ_r (º)
						c_{cu} (MPa)	ϕ_{cu} (º)	
Siliciclastic Flysch	*Minimum*	20.7	0.14	0.04	1.24	0.2	35.0	18.0
	Maximum	28.5	76.25	12.47	4.38	19.9	44.0	30.0
	Average	26.4	24.83	8.43	2.95	10.0	39.5	23.0
	Std. dev.	1.4	18.08	3.56	1.30	13.9	6.4	9.7
Calcareous Flysch	*Minimum*	24.5	6.03	4.55	0.91	0.2	42.0	23.0
	Maximum	27.6	49.87	9.83	4.55	16.9	57.0	37.0
	Average	26.4	22.89	6.49	2.74	8.6	49.0	30.0
	Std. dev.	0.9	14.10	2.40	1.76	11.3	3.2	11.8

Table 3

Table 3. Geomechanical characterization results.

Point	Geological flysch unit	σ_{ci}	RQD	RMR_B	GSI	m_i	m_b	s	a	σ_c	σ_{tm}	σ'_{cm}	E_m
1	Siliciclastic	37.7	50	60	54	7	1.35	0.0060	0.504	2.86	-0.17	6.10	7729.8
2	Siliciclastic	42.4	45	62	55	8	1.60	0.0067	0.504	3.41	-0.18	7.46	8683.3
3	Siliciclastic	40.0	55	57	52	7	1.26	0.0048	0.505	2.70	-0.15	6.18	7096.3
4	Siliciclastic	42.3	65	61	48	7	1.09	0.0031	0.507	2.27	-0.12	5.96	5796.6
5	Siliciclastic	38.6	63	64	47	7	1.05	0.0028	0.507	1.95	-0.10	5.32	5227.5
6	Siliciclastic	40.1	65	47	35	11	1.08	0.0007	0.516	0.97	-0.03	5.23	2670.4
7	Siliciclastic	41.1	54	58	43	8	1.04	0.0018	0.509	1.63	-0.07	5.51	4284.7
8	Siliciclastic	32.5	48	59	38	9	0.98	0.0010	0.513	0.95	-0.03	4.11	2857.2
9	Siliciclastic	42.5	72	69	58	14	3.12	0.0094	0.503	4.06	-0.13	10.32	10332.2
10	Siliciclastic	43.2	69	72	63	9	2.40	0.0164	0.502	5.48	-0.29	9.69	13891.3
11	Siliciclastic	26.5	64	60	49	7	1.13	0.0035	0.506	1.50	-0.08	3.82	4859.8
12	Siliciclastic	32.1	63	55	47	7	1.05	0.0028	0.507	1.62	-0.08	4.42	4767.1
13	Siliciclastic	37.8	53	45	38	8	0.87	0.0010	0.513	1.10	-0.04	4.51	3081.4
14	Calcareous	23.5	20	43	37	8	0.84	0.0009	0.514	0.64	-0.02	2.74	2293.7
15	Calcareous	21.5	21	27	20	9	0.52	0.0001	0.544	0.17	-0.01	1.65	824.5
16	Calcareous	22.3	23	21	18	7	0.37	0.0001	0.550	0.15	-0.01	1.39	748.4
17	Calcareous	30.0	35	28	25	15	1.03	0.0002	0.531	0.36	-0.01	3.54	1298.8
18	Calcareous	27.4	45	41	36	11	1.12	0.0008	0.515	0.70	-0.02	3.66	2338.2
19	Siliciclastic	50.2	70	74	69	3	0.99	0.0319	0.501	8.92	-1.62	9.46	21152.0
20	Siliciclastic	51.3	77	74	69	11	3.64	0.0319	0.501	9.12	-0.45	14.56	21382.5
21	Calcareous	25.6	26	23	20	11	0.63	0.0001	0.544	0.20	-0.01	2.19	899.7
22	Calcareous	30.1	18	26	18	8	0.43	0.0001	0.550	0.20	-0.01	2.01	869.5
23	Calcareous	31.0	43	49	41	8	0.97	0.0014	0.511	1.09	-0.04	3.97	3316.51
24	Calcareous	30.5	65	62	54	7	1.35	0.0060	0.504	2.32	-0.14	4.94	4952.6
25	Calcareous	17.5	29	37	19	7	0.39	0.0001	0.547	0.13	-0.01	1.13	702.3
26	Calcareous	12.3	36	45	38	7	0.77	0.0010	0.513	0.36	-0.02	1.37	1757.7
27	Siliciclastic	13.4	60	66	58	7	1.56	0.0094	0.503	1.28	-0.08	2.39	5801.7
28	Calcareous	20.5	24	23	17	8	0.41	0.0001	0.553	0.12	-0.01	1.32	677.4
29	Calcareous	20.0	25	44	37	8	0.84	0.0009	0.514	0.55	-0.02	2.33	2116.0
30	Calcareous	19.8	39	45	36	15	1.53	0.0008	0.515	0.51	-0.01	3.09	1987.6
31	Calcareous	23.4	32	47	42	11	1.39	0.0016	0.510	0.87	-0.03	3.58	3052.2
32	Siliciclastic	22.6	55	62	57	8	1.72	0.0084	0.504	2.04	-0.11	4.17	7113.0
33	Siliciclastic	32.1	50	63	56	8	1.66	0.0075	0.504	2.73	-0.14	5.78	8003.0

Notation: *RQD: Rock Quality Index, in %;* σ_{ci}*: uniaxial compression strength of the intact rock, in MPa;* RMR_B*: Basic Rock Mass Rating (Bieniaswki, 1989); GSI: Geological Strength Index (Hoek, 2000; Marinos and Hoek, 2001);* m_i, m_b, *s, a: parameters of the Hoek-Brown model (Hoek et al., 2002);* σ_c*: uniaxial compression strength of the rock mass, in MPa;* σ_{tm}*: rock mass tensile strength, in MPa;* σ'_{cm}*: rock mass strength, in MPa* E_m*: Young modulus of the rock mass, in MPa.*

Table 4. Rock mass classes description and estimated Hoek-Brown parameters (Hoek and Brown, 1997; Hoek *et al*., 2002; Marinos and Hoek, 2001) for flysch deposits according to Morales *et al*. (2004).

Rock mass class	**Description**	**m_b**	**s**	**a**
Class 1	Very competent rock masses, made up of high compressive strength (σ_{ci}) materials, massive or thick-bedded. The discontinuities affecting the rock mass do not constitute persistent and regular sets of weakness (GSI over 50). They are generally either very compact sandstone and limestone or materials of igneous origin.	4.298	0.02	0.502
Class 2	Rock masses consisting of highly competent materials, with σ_{ci} values similar to class 1, affected by wide-spaced discontinuity sets (GSI values under 50). The rocks are basically thick-bedded blocky sandstones, limestones and igneous materials.	1.942	0.0035	0.506
Class 3	The materials making up the rock mass have a σ_{ci} of less than 30 MPa and relatively high GSI values (from 35 to 45). They are generally very competent marls or claystones.	1.793	0.005	0.520
Class 4	Rock masses with a GSI from 25 to 40 and a medium-high σ_{ci} value (over 25 MPa). This group largely consists of rock masses in which competent materials, predominant (generally sandstone or limestone) and alternate with less competent layers (argillaceous marls, siltstone or claystone).	1.042	0.0007	0.517
Class 5	Rock masses consisting of materials with a σ_{ci} of less than 25 MPa, basically marls and competent siltstone. The discontinuity rating is relatively high (GSI between 30 and 40).	0.756	0.001	0.513
Class 6	These are rock masses made up of materials of medium compressive strength (σ_{ci} over 20 MPa) or equal amounts of layers of very different strength. The GSI value is between 25 and 35.	0.529	0.0005	0.520
Class 7	Rock masses consisting of siltstone and alternations with predominant siltstone (σ_{ci} under 20 MPa). Their discontinuity rating is high, with significant weathering (GSI ranging from 25 to 35).	0.459	0.003	0.526
Class 8	These are weak rock masses as a result of intense jointing or because the rock material itself has a low strength. This class also includes very weathered rock masses. The GSI is under 27 and the σ_{ci} is no more than 15 MPa.	0.320	0.0002	0.536

Table 5

Table 5. Geomechanical characterization average values.

Geological flysch unit	σ_{ci}	**RQD**	RMR_B	**GSI**	σ_c	σ_{tm}	σ'_{cm}	E_m
Siliciclastic Flysch								
Average	37.0	59.9	61.6	52.0	3.03	-0.22	6.39	8040.5
Std. deviation	9.4	9.1	8.0	9.9	2.47	0.36	2.95	5556.5
Calcareous Flysch								
Average	23.7	32.1	37.4	30.5	0.56	-0.02	2.59	23.7
Std. deviation	5.4	12.4	12.1	11.6	0.57	0.03	1.16	5.4

Notation: *RQD: Rock Quality Index, in %;* σ_{ci}*: uniaxial compression strength of the intact rock, in MPa;* RMR_B*: Basic Rock Mass Rating (Bieniaswki, 1989); GSI: Geological Strength Index (Hoek, 2000; Marinos and Hoek, 2001);* σ_c*: uniaxial compression strength of the rock mass, in MPa;* σ_{tm}*: rock mass tensile strength, in MPa;* σ'_{cm}*: rock mass strength, in MPa* E_m*: Young modulus of the rock mass, in MPa.*